

Vector-borne epidemics driven by human mobility

David Soriano-Paños^{1,2}, Judy Heliana Arias-Castro³, Hector J. Martínez³, Sandro Meloni⁴, and Jesús Gómez-Gardeñes^{1,2,*}

¹GOTHAM Lab., Institute for Biocomputation and Physics of Complex Systems (BIFI), University of Zaragoza, 50018 Zaragoza, Spain

²Departament of Condensed Matter Physics, University of Zaragoza, 50009 Zaragoza, Spain

³Department of Mathematics, Universidad del Valle, 760032 Santiago de Cali, Colombia

⁴Instituto de Física Interdisciplinar y Sistemas Complejos IFISC (CSIC-UIB), Campus UIB, 07122 Palma de Mallorca, Spain

*gardenes@unizar.es

ABSTRACT

Vector-borne epidemics are the result of the combination of different factors such as the crossed contagions between humans and vectors, their demographic distribution and human mobility among others. The current availability of information about the former ingredients demands their incorporation to current mathematical models for vector-borne disease transmission. Here, relying on metapopulation dynamics, we propose a framework whose results are in fair agreement with those obtained from mechanistic simulations. This framework allows us to derive an expression of the epidemic threshold capturing with high accuracy the conditions leading to the onset of epidemics. Driven by these insights, we obtain a prevalence indicator to rank the patches according to the risk of being affected by a vector-borne disease. We illustrate the utility of this epidemic risk indicator by reproducing the spatial distribution Dengue cases reported in the city of Santiago de Cali (Colombia) from 2015 to 2016.

Introduction

The explosive dissemination of Zika virus across the Americas has been one of the major concerns of public health organizations across the world in the recent years¹. Zika's global threat is, unfortunately, the last example of the extremely rapid dissemination of mosquito-borne flaviviruses over the past two decades. From Dengue to Zika, through West Nile and Chikungunya viruses, more than one billion people are infected and more than one million people die from vector-borne diseases (VBD) every year². According to the World Health Organization (WHO), VBD are responsible of one sixth of the illness worldwide and more than half of human population live in risk areas for these diseases³. Moreover, the threat of new emergent VBD in tropical and ecuatorial regions progressively span across more temperate areas as a byproduct of climate change. As temperature rises, the areas that are conducive to mosquitoes expand, meaning more opportunities for VBD to spread⁴. For the case of Malaria, an increase of global temperature of 2-3 degrees would rise the population at risk by several hundred million people while, in the case of Dengue, the population at risk would pass from 1-2 billion people in 1990 to 5-6 billion in 2085⁵⁻⁷.

The lack of efficient vaccines constitutes another significant bump on the road of facing flaviviruses epidemics. Despite the efforts for finding effective immunization means to slow down the advance of *Aedes*-borne viruses, the most common way for preventing outbreaks is the use of pesticides, larvivorous fishes or Wolbachia bacteria, all of them directly acting over the vector⁸. The use of geolocalized control strategies, however, seems not to be an effective prevention strategy when facing the threat of a global-scale pandemic. On the contrary, the fast transcontinental movement of VBD demands a coordinated action of the involved actors for the efficient use of local control means. This implies taking into account that those populations at risk are not isolated and, as for human-human transmission diseases⁹, human mobility plays a key role in the spread of VBD across different populations¹⁰. In this sense, over the last decades, the increasing use and efficiency of transportation means have led to an explosion of human mobility, including urban, regional and long-range displacements¹¹⁻¹⁵. Despite the social and economical benefits, the expansion of human mobility networks produced, as a byproduct, the speed up of epidemic waves and the emergence of correlated outbreaks in far away regions. For this reason, incorporating human mobility into disease transmission models has become a must when proposing mathematical frameworks aimed at capturing the contagions patterns observed in actual epidemic scenarios.

Metapopulation models, originally proposed in the field of ecology¹⁶⁻¹⁸, enable the mixing of mobility and contagion dynamics into a single formulation. These models can be described as networks in which nodes account for geographic locations (such as neighborhoods in cities, cities within countries, etc), *i.e.* subpopulations where large collectivities live and interact. In addition, the links of the network represent (and quantify) trips made by individuals between different subpopulations.

From the first studies making use of metapopulations for the study of infectious diseases transmission^{19,20}, the field has advanced both in its theoretical grounds^{21–26} and its use for large-scale agent-based simulations^{27–29}. The latter approach incorporates many realistic aspects of human interactions with the goal of being useful for making epidemic forecast and the design of efficient prevention policies. On the other hand, the theoretical part has been spurred by the increasing spatio-temporal resolution of current data gathering techniques and many efforts have been devoted to bridge the gap between theory and realistic models during the last years³⁰. First attempts in this direction involved displacement kernels^{31,32} to model a local range of movement around an area that, in the last years, lead the way to the inclusion of more sophisticated mobility patterns, such as the commuting nature of human mobility^{33–36}, the high order memory of human displacements³⁷, or the coexistence of different transportation behaviors³⁸. These sophisticated theories allow to capture the temporal and geographical spread of diseases while providing insights about the mechanisms driving the observed patterns.

In the case of VBD the use of metapopulation models has been recently fostered due to recent outbreaks such as Zika and Chikungunya. This way, epidemic models for VBD transmission have abandoned mean-field and well mixed hypothesis to consider patchy environments subjected to human flows. On the theoretical side, and pretty much as for metapopulations models of human-human transmission diseases, the frameworks rely on important assumptions that allow its analytical study. One of these assumptions is to consider the random diffusion of humans across patches^{39–41} or displacement kernels⁴² instead of realistic mobility patterns. On the other hand, when actual ingredients of human mobility, such as its recurrent nature, are taken into account both random diffusion^{43,44} and displacement kernels models⁴⁵ fail in providing insights about the role that real mobility networks play on the transmission of VBD. Thus, metapopulation theories are still far from incorporating the many aspects influencing the onset of VBD outbreaks and lack the predictive power provided by data-driven agent-based simulations^{46,47}.

The main goal of this work is to provide a benchmark that allows the study of large-scale vector-borne epidemics in a unified way and, more importantly, enabling the test of coordinated control strategies at the light of available data about vector incidence together with human demography and mobility datasets. To this aim, we first elaborate a metapopulation model for the transmission of VBD that allows us to derive the conditions under which epidemics take place. The analytical expression of the epidemic threshold is revealed by a matrix encoding the probability of crossed infections between humans and vectors of different subpopulations. Importantly, the spectral analysis of this matrix reveals the risk associated to each patch, pointing out those subpopulations triggering the epidemic onset. We confirm these results by testing synthetic metapopulations and a real case, the city of Cali (Colombia). To round off, taking advantage of the theoretical insights and analytical expressions provided by the formalism, we propose a metric capturing the risk associated to each patch. We implement this metric in the city of Cali obtaining a very good agreement between the estimated risk and the actual distribution of Dengue incidence across districts, highlighting the important role of recurrent human mobility patterns for explaining the spatial dissemination of VBD.

Results

Metapopulation model for VBD transmission

In the following, we will focus on the description of a vector-borne contagion dynamics in a complex metapopulation. To this aim, we consider a set of N populations or patches in which contagion processes occur. In particular, we consider that the dynamic inside each patch is governed by the Ross-Macdonald (RM) model, as it captures the essential ingredients involved in VBD that do not confer immunity to reinfections such as Dengue. Other models including different disease-specific contagion patterns, such as human-human contagions in Zika^{48,49}, can be easily accommodated in the introduced framework. The relevant variables of the RM dynamics are: (i) the fraction of infected humans at time t , $\rho^H(t)$, and (ii) the fraction of vectors infected at time t , $\rho^M(t)$. The evolution of these two variables is given as a product of the elementary processes described in Fig. S1a. Namely, susceptible humans become infected with probability λ^{MH} after being bitten by an infected vector whereas healthy vectors become infectious with probability λ^{MH} when interacting with an infected human. In addition, we assume that each vector makes a number of β contacts with (healthy or infected) humans. This way, no human-human or vector-vector direct infections are allowed. Finally, infected humans become susceptible with probability μ^H , while (healthy or infected) vectors die with probability μ^M , being replaced by newborn healthy ones.

Although the RM dynamics captures the elementary contagion processes taking place inside each population, the dynamical evolution of each patch depends strongly on the others, since they are not isolated. On the contrary, many individuals with residence in one subpopulation may visit others during, for instance, their daily commutes to other geographical locations. On the other hand, the mobility of vectors is rather limited, hence they are assumed not to move from their original population. This assumption is valid for many VBD such as Dengue, Zika or Chikungunya since their carriers, *Aedes* mosquitoes, typically fly an average of 400 meters⁵⁰. Thus, it is the mobility of infectious individuals (who pass the diseases to healthy vectors living in distant subpopulations) what triggers the propagation of local disease outbreaks across the whole system. To characterize the mobility of individuals we denote each population as a node of a graph. Each node i has a population of n_i individuals and m_i vectors and, importantly, they may be different from one population to the other, as they are derived from the demographic

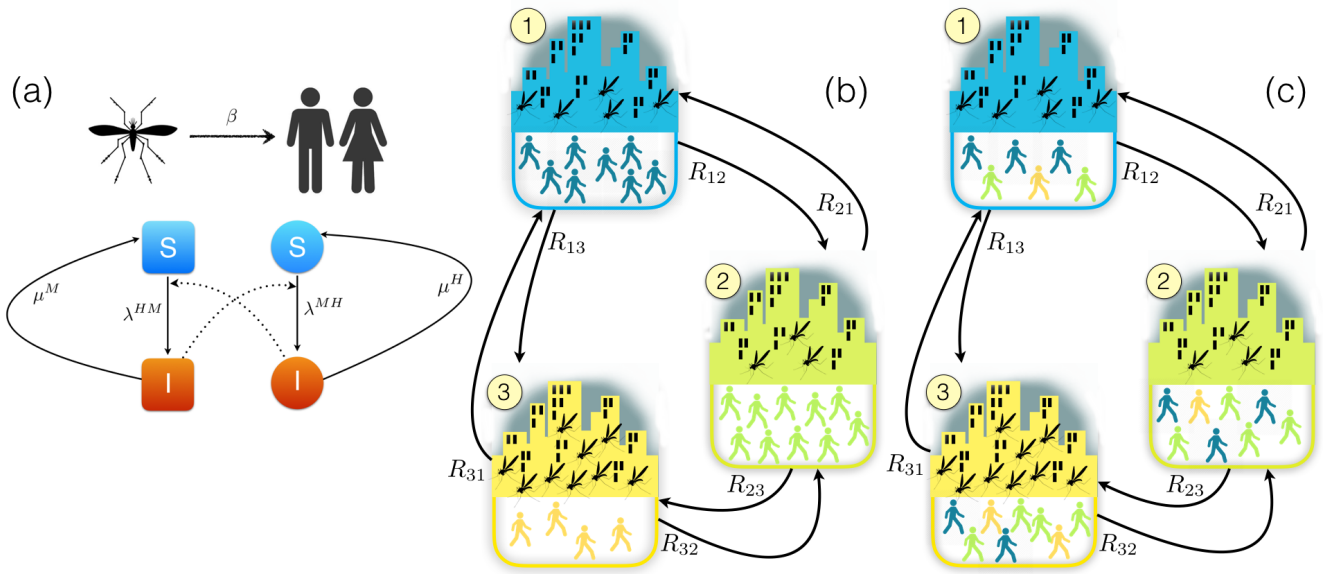


Figure 1. Ross-Macdonald model and metapopulation approach. (a) Schematic representation of the processes described in the RM model. Relevant parameters are: (i) the probability that an infected vector transmits the disease to a healthy individual, λ^{MH} , (ii) the probability that an infected human transmits the disease to a healthy vector, λ^{HM} , (iii) the feeding rate of vectors β , (iv) the probability that an infected human recovers, μ^H , and (v) the mortality rate of vectors, μ^M . In (b) and (c) we show schematically the two basic stages of each Monte Carlo step in our metapopulation approach. As shown in (b), individuals are associated to one of the 3 nodes of a network. Namely, starting from the subpopulation in the top (1) and following clockwise we have populations composed of 8, 10 and 4 humans with 5, 3 and 9 vectors respectively. Once the movement has been done [see panel (c)] individuals mix and, consequently, the instant populations of humans at each node change to 6, 8 and 8. The RM dynamics then takes place among the individuals and vectors coexisting at that moment in the same subpopulation. Finally, after these interactions, the individuals go back to their respective associated nodes and the configuration is again the one of panel (b). Note that we consider that vectors do not move from their corresponding node.

partition of the population and the observed vector prevalence in each patch. It is important to recall that each individual is associated to one subpopulation, say i , considered as her residence. This way, the population n_i of the patch i is the number of individuals whose residence is node i . In its turn, nodes are connected in pairs forming a complex weighted and directed network encoded in an adjacency matrix \mathbf{R} , whose entries R_{ij} account for the the probability that a trip departing from patch i has as destination population j (see Figure S1b). Matrix \mathbf{R} can be computed from the observed number of trips between each pair of nodes (i, j) , W_{ij} , as:

$$R_{ij} = \frac{W_{ij}}{\sum_{j=1}^N W_{ij}}. \quad (1)$$

Thus, matrix \mathbf{R} encodes the information provided by mobility datasets .

The former two dynamical processes at work –RM dynamics and human movements– interplay in each time step of the metapopulation dynamics as follows. We start with a small fraction of infected humans and/or vectors. The initial quantity, being small, can be homogeneously distributed across the populations or localized in one or few nodes in case of being interested in determining those patches boosting epidemic spreading in its early stage. Once the initial infectious seed has been placed, the simulation steps per unit time are the following:

- At each time step, t , healthy agents decide to move from their residence with probability p or remaining in it with probability $(1 - p)$. Moreover, as symptoms associated to some VBD are severe, we also include the possibility of re-scaling the infected agents' mobility to αp with $\alpha \in [0, 1]$.
- If an agent leaves her residence, say i , she goes to a different subpopulation chosen among those connected to i . The choice is dictated by matrix \mathbf{R} in Eq. (1), being R_{ij} the probability of moving from i to subpopulation j .

- Once all the individuals have been placed in the patches (see Fig. S1.c), humans and vectors that are currently at the same patch interact as dictated by the RM model. This way, both humans and vector update their dynamical states (Susceptible or Infected as shown in Fig. S1.a) as a result of the contagion and recovery processes.
- Once the epidemic state of the agents have been updated, each individual moves back to her residence and the process starts again for time $t + 1$.

Markovian Formulation

Once defined the basic steps of the mechanistic simulations, we now tackle the mathematical formulation of the processes described above. To this aim, for each patch i ($i = 1, \dots, N$) we have 2 variables: the probabilities that humans with residence in i , $\rho_i^H(t)$, and vectors associated to i , $\rho_i^M(t)$, are infectious at time t respectively. These $2N$ variables evolve according to the following Markovian equations:

$$\rho_i^H(t+1) = \rho_i^H(t)(1 - \mu^H) + (1 - \rho_i^H(t))I_i^H(t), \quad (2)$$

$$\rho_i^M(t+1) = \rho_i^M(t)(1 - \mu^M) + (1 - \rho_i^M(t))I_i^M(t), \quad (3)$$

where $I_i^H(t)$ and $I_i^M(t)$ account for the probability that a healthy human with residence in subpopulation i and a healthy vector associated to i are infected at time t respectively. The former infection probability reads:

$$I_i^H(t) = (1 - p)P_i^H(t) + p \sum_{j=1}^N R_{ij}P_j^H(t), \quad (4)$$

where $P_i^H(t)$ is the probability that an agent placed in population i at time t is infected. This probability can be written as:

$$P_i^H(t) = 1 - \left(1 - \lambda^{MH} \rho_i^M \frac{1}{n_i^{eff}(\rho_H(t), \alpha, p)} \right)^{\beta m_i}. \quad (5)$$

Finally, $n_i^{eff}(\rho_H(t), \alpha, p)$, which is the number of humans placed in (but not necessarily resident in) population i can be expressed as:

$$\begin{aligned} n_i^{eff}(\rho_H(t), \alpha, p) &= [1 - p(1 - (1 - \alpha)\rho_i^H(t))] n_i \\ &+ p \sum_{j=1}^n R_{ji} (1 - (1 - \alpha)\rho_j^H(t)) n_j. \end{aligned} \quad (6)$$

In the same fashion, the expression for $I_i^M(t)$ in Eq. (3) reads:

$$I_i^M(t) = 1 - \left(1 - \lambda^{HM} \frac{i_i^{eff}(t)}{n_i^{eff}} \right)^{\beta} \quad (7)$$

where $i_i^{eff}(t)$ is the number of infected humans placed in population i at time t :

$$i_i^{eff}(t) = (1 - \alpha p) n_i \rho_i^H(t) + \alpha p \sum_{j=1}^N R_{ji} n_j \rho_j^H(t). \quad (8)$$

The above equations describe the time evolution for the VBD incidence, $\vec{\rho}^H(t) = \{\rho_i^H(t)\}$ and $\vec{\rho}^M(t) = \{\rho_i^M(t)\}$, in a collection of connected patches with arbitrary demographic, \vec{n} , and vector, \vec{m} , distribution. They enable, by integrating the equations starting from a given initial condition $\vec{\rho}^H(0)$ and $\vec{\rho}^M(0)$, to monitor the geographical spread of VBD and to analyze the stationary incidence of the diseases across patches, while the global incidence of the disease can be calculated as the fraction of infected humans in the entire system $\rho^H = \frac{\sum_i \rho_i^H n_i}{\sum_i n_i}$. The accuracy of Eqs. (2)-(3) has been tested with the results derived from mechanistic simulations in synthetic metapopulations (see Methods). As shown in Figures S3 and S4 of the SI, the perfect agreement found both for stationary solutions and the spatio-temporal evolution points out the validity of the Markovian formulation.

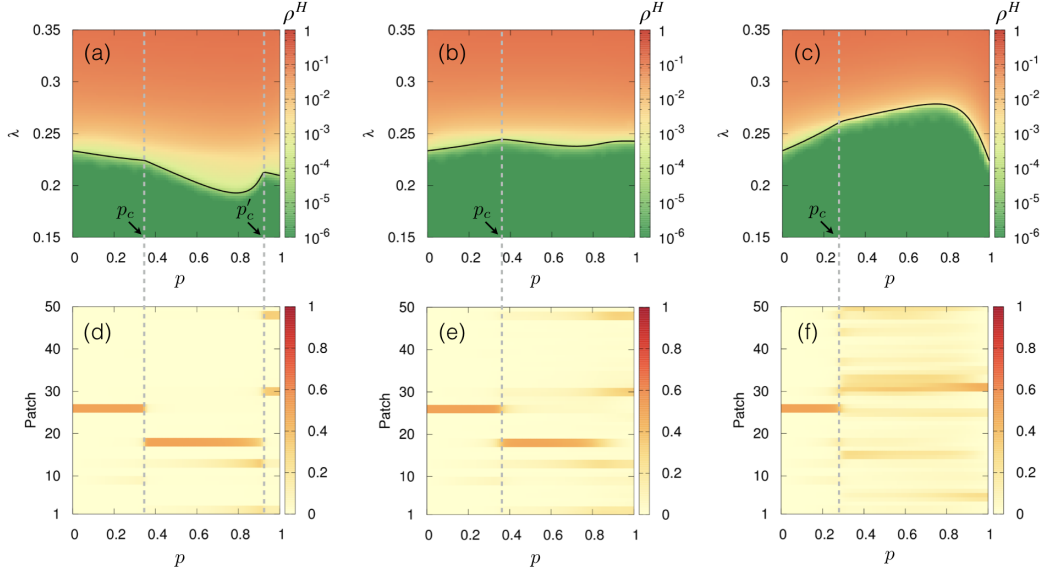


Figure 2. Epidemic threshold and evolution of the leading eigenvector of matrix $\tilde{\mathbf{M}}\mathbf{M}$. Panels (a)-(c) in the top show three epidemic diagrams $\rho^H(p, \lambda)$ in a synthetic metapopulation of $N = 50$ patches. Each panel corresponds to a different re-scaling value (α) for the mobility of infected humans, namely: (a) $\alpha = 0$, (b) $\alpha = 0.5$ and (c) $\alpha = 1$. In addition, we have set $\lambda^{HM} = \lambda^{MH} = \lambda$ while the rest of the RM parameters are: $\mu^H = 0.3$, $\mu^M = 0.3$, and $\beta = 1.0$. The color code show the incidence ρ^H as obtained from agent-based simulations while the solid curve represent the prediction for the epidemic threshold, λ_c , calculated from Eq. (14). The bottom panels (d)-(f) show the evolution, as a function of p , of the N components of the eigenvector of matrix $\mathbf{M}\tilde{\mathbf{M}}$ corresponding to maximum eigenvalue $\Lambda_{max}(\mathbf{M}\tilde{\mathbf{M}})$.

Estimation of the epidemic threshold

The validation of Eqs. (2)-(3) offers the possibility of saving computational costs by integrating the $2 \times N$ Markovian equations instead of performing lengthy agent-based simulations. However, the advance behind Eqs. (2)-(3) is that they also allow for deriving metrics and analytical results about the dynamical behavior of VBD in large metapopulations. A relevant quantity that can be analyzed is the epidemic threshold, *i.e.*, those conditions that turns the epidemic state into a stable solution of Eqs. (2)-(3). To address this, we suppose that the infection probabilities of humans and vectors in the stationary state are very small: $\rho_i^H = \varepsilon_i^H \ll 1$, $\rho_i^M = \varepsilon_i^M \ll 1 \forall i$. This assumption allows us to linearize Eqs. (2)-(3) and, after some algebra (see SI), the stationary solutions for the infection probabilities of humans, $\vec{\varepsilon}^H$ read:

$$\vec{\varepsilon}^H = \frac{\beta^2 \lambda^{MH} \lambda^{HM}}{\mu_M \mu_H} (\tilde{\mathbf{M}}\mathbf{M}) \vec{\varepsilon}^H, \quad (9)$$

where the entries of matrices \mathbf{M} and $\tilde{\mathbf{M}}$ (see SI for their derivation) take the following form:

$$M_{ij} = \left(p R_{ij} \frac{m_j}{\tilde{n}_j^{eff}} + (1-p) \delta_{ij} \frac{m_i}{\tilde{n}_i^{eff}} \right), \quad (10)$$

$$\tilde{M}_{ij} = \left(\alpha p R_{ji} \frac{n_j}{\tilde{n}_i^{eff}} + (1-\alpha p) \delta_{ij} \frac{n_i}{\tilde{n}_i^{eff}} \right), \quad (11)$$

where \tilde{n}_i^{eff} is defined as $\tilde{n}_i^{eff} = n_i^{eff}(0, \alpha, p)$. Note that the form of the elements of these two matrices depends on both the mobility properties (p , \mathbf{R}) and the demographic distribution of both agents and vectors (\vec{n} , \vec{m}).

From Eq. (9) it is clear that nontrivial solutions for $\vec{\varepsilon}^H$ correspond to the eigenvectors of matrix $\tilde{\mathbf{M}}\mathbf{M}$. Specifically, given a metapopulation defined by \vec{n} , \vec{m} , \mathbf{R} and p , the stationary solutions with infinitesimal incidence correspond to eigenvectors of $\tilde{\mathbf{M}}\mathbf{M}$ whose eigenvalues fulfil:

$$\Lambda_i = \frac{\mu^M \mu^H}{\beta^2 \lambda^{MH} \lambda^{HM}}, \quad (12)$$

Under these conditions, the maximum eigenvalue $\Lambda_{max}(\tilde{\mathbf{M}}\tilde{\mathbf{M}})$ encodes the combination of the RM parameters that corresponds to the epidemic threshold, namely:

$$\frac{\beta^2 \lambda^{MH} \lambda^{HM}}{\mu^M \mu^H} \Lambda_{max} = 1 . \quad (13)$$

The former equation reveals the minimum infectivities, either λ^{HM} or λ^{MH} , that trigger the epidemic outbreak. To derive a simple critical infectivity one can set $\lambda^{MH} = \delta \lambda^{HM}$, so that:

$$\lambda_c^{MH} = \sqrt{\frac{\mu_H \mu_M}{\delta \beta^2 \Lambda_{max}(\tilde{\mathbf{M}}\tilde{\mathbf{M}})}} \quad (14)$$

To test the validity of Eq. (14) we have carried out extensive numerical simulations in synthetic metapopulations (see the SI for a detailed description) considering $\lambda^{MH} = \lambda^{HM} = \lambda$. The top panels in Fig. 2 show the epidemic diagrams $\rho^H(p, \lambda)$ by computing the fractions of humans infected, ρ^H , as a function of λ and p . From these diagrams it becomes clear that, for each value of p , there exist a critical value λ_c so that for $\lambda > \lambda_c$ the epidemic phase appears. The border of this region (solid curves in Fig. 2.a-c)) is the function $\lambda_c(p)$ calculated with Eq. (14), showing an excellent agreement with the results from numerical simulations.

Abrupt transitions of leading patches

Apart from the agreement between Eq. (14) and the numerical simulations, the evolution of the epidemic threshold, $\lambda_c(p)$, reported in the three upper panels points out a non-trivial dependence with the degree of human mobility. Contrary to what naively expected, human mobility can be detrimental to epidemics, as clearly illustrated in the panels for $\alpha = 0.5$ and $\alpha = 1.0$. This counterintuitive effect of mobility was already found for SIR and SIS diseases in networked metapopulations³⁶ as a result of the redistribution of the effective populations across patches due to mobility. In the case of VBD, this process corresponds to an homogeneization of the effective ratios between vectors and humans so that a high risk patch with large $\gamma_i = m_i/n_i$ tends to decrease its effective value due to the increase of n_i^{eff} , Eq.(6), caused by the mobility.

A more striking phenomenon reported in the epidemic diagrams of Fig. 2 is revealed by the sharp variations in the slope of the curves $\lambda_c(p)$. These abrupt changes are the product of collisions between the two maximum eigenvalues of matrix $\mathbf{M}\mathbf{M}$ as p varies. This way, the two maximum eigenvalues interchange their order at some critical mobility value p_c . These collisions do not have an strong impact in the epidemic threshold since the function $\lambda_c(p)$ is continuous. However, they are the fingerprint of a sudden change in the form of the eigenvector corresponding to the maximum eigenvalue, \vec{v}_{max} , of matrix $\tilde{\mathbf{M}}\tilde{\mathbf{M}}$. This abrupt transition is of utmost importance since the components of \vec{v}_{max} encode the most important patches driving the unfolding of the epidemics.

Let us recall that matrix $\tilde{\mathbf{M}}\tilde{\mathbf{M}}$ incorporates the demographic information, \vec{n} , the mobility patterns, \mathbf{R} and the vector distribution, \vec{m} , having as unique parameter the degree of mobility p . Thus, for each value of p the spectral analysis of $\tilde{\mathbf{M}}\tilde{\mathbf{M}}$ gives us the epidemic threshold λ_c and the distribution of patches triggering the epidemic onset in the components of \vec{v}_{max} . The evolution of the components of \vec{v}_{max} as a function of p is shown in the bottom panels, (d-f), of Fig. 2. From these plots it becomes clear that the discontinuities of the slope of $\lambda_c(p)$ correspond to abrupt changes in the form of \vec{v}_{max} . Namely, in the three cases patch number 26 is the one causing the epidemic onset for $p = 0$ and $p \ll 1$. This is obvious since patch 26 is the one with largest ratio $\gamma_i = m_i/n_i$ in the synthetic metapopulation. However, as p increases, the leading patch changes, being replaced by patch 18 in the case of $\alpha = 0$ (d) and $\alpha = 0.5$ (e) while for $\alpha = 1$ (f) the leading patch is replaced by a collection of them. Remarkably, the case $\alpha = 0$ shows a second abrupt transition at $p'_c \simeq 0.92$. These abrupt changes point out that containment strategies targeting a certain neighborhood can change sharply from efficient to useless due to changes in human mobility, as confirmed in the SI.

Assessing the epidemic risk of patches with $\tilde{\mathbf{M}}\tilde{\mathbf{M}}$

Spurred by the ability of the Markovian formalism to capture the dynamics of VBD and the insights provided by the spectral properties of matrix $\mathbf{M}\mathbf{M}$ for identifying the areas triggering the onset of epidemics, we move one step further and evaluate the epidemic risk associated to each patch. To this aim, we propose a theory-driven prevalence indicator which serves as a proxy to determine the most exposed areas to the spread of VBD.

For this purpose, let us analyze the elements of the matrices \mathbf{M} and $\tilde{\mathbf{M}}$, defined in Eqs. (10)-(11). From these equations we realize that the elements M_{ij} (\tilde{M}_{ij}) contain all the possible microscopic contagion processes from vectors (humans) associated to patch j to humans (vectors) associated to i . Therefore, it is possible to estimate the effective number of human-human contagions mediated by vectors that an individual from subpopulation i receives from those with residence in j . This quantity, denoted as C_{ij} , can be obtained taking into account all the possible infection pathways connecting humans in patch j to those of

i as described in Eq. 15. Those infections may take place in three possible ways: (i) an infected individual from patch j visits patch i and infect a vector that will later pass the disease to a resident of patch i ; (ii) a resident of patch j infects a vector and a healthy human traveling to j from i gets infected; (iii) both the infected individual from j and the healthy individual from i travel to a contiguous third patch k where the infection takes place mediated by a vector.

$$C_{ij} = \sum_{k=1}^N M_{ik} \widetilde{M}_{kj}. \quad (15)$$

Finally, to make predictions about the impact of the disease on a geographical area, i , we must account for all the possible infections from each patch of the metapopulation and to weight the resulting number by the population of i . This way, the epidemic risk indicator for each patch i , in the following denoted as ER_i , can be defined as:

$$ER_i = n_i \sum_{j=1}^N C_{ij} = n_i \sum_{j=1}^N \left(\widetilde{\mathbf{M}\mathbf{M}} \right)_{ij}. \quad (16)$$

The evaluation of ER_i , as defined above, can be done directly without the need of neither numerical simulations nor making the integration of the Markovian equations. In fact, once data about demography, vector distribution and mobility patterns are available, one can estimate the epidemic risk of each subpopulation. In the SI we show the validation of the risk indicator for the synthetic metapopulations by comparing the values ER_i with the disease incidence as obtained from the mechanistic

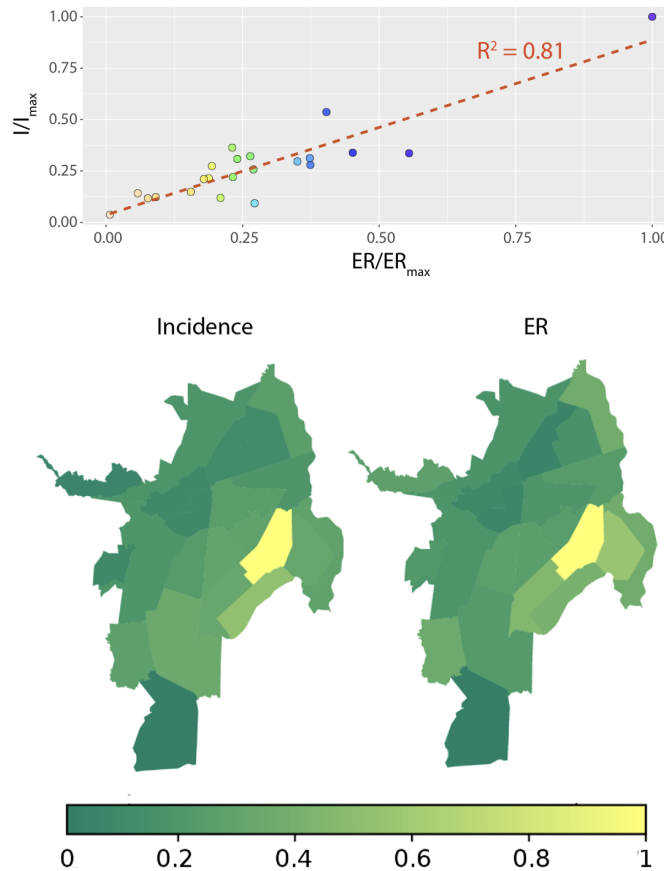


Figure 3. Real Dengue incidence versus estimated epidemic risk in the city of Cali (Colombia). Top: Normalized epidemic risk (ER/ER_{max}) versus normalized Dengue incidence (I/I_{max}) for each of the 22 districts of Cali. Color encodes the Epidemic Risk, from the lower (yellow) to the highest (blue). The correlation between the two variables yields a coefficient of determination of $R^2 = 0.81$. Bottom: Spatial distributions of the normalized Dengue incidence in the city of Cali (left) and the normalized epidemic risk (right) according to Eq. (16). The parameters concerning agents' mobility have been set to $(p, \alpha) = (0.36, 0.75)$ (see SI for more details).

simulations. The fair agreement (coefficient of determination $R^2 = 0.95$) between our indicator and the results from numerical simulations allows us to rank the patches according to their exposure to VBD without the need of performing computationally expensive simulations or integrating an large set of Markovian equations.

A real metapopulation: Santiago de Cali (Colombia)

To validate further the Epidemic Risk measure we now move to a real metapopulation, the city of Santiago de Cali (Colombia). With a population of more than 2 millions of inhabitants, it offers the possibility of comparing our predictions in a scenario for which severe epidemic outbreaks of VBD are recurrently found. In particular, due to its location and climate, Cali is a Dengue endemic area in which records of the historical incidence of this disease are available for comparison. To this aim, we collected demographic and mobility datasets¹⁰ whereas vectors abundance across districts was obtained from entomological reports made yearly by the local authorities⁵².

With this information at hand, and using Eq. (16), we assign the epidemic risk of each of the 22 districts in which the city is divided. These values are compared to the observed Dengue incidence across the 22 patches during the period 2015-2016⁵³ (details in the SI). In Fig. (3) we show this comparison by normalizing the values of both epidemic risk and Dengue incidence by their maximum observed value (in both cases that of district 13). In particular, we find a coefficient of determination of $R^2 = 0.81$, indicating that the proposed prevalence indicator is able to capture the spatial distribution of Dengue cases across the city. On more general grounds, this agreement points out that given the demography, the commuting patterns and the spatial distribution of vectors across a given population, one can use Eq. (16) to identify areas where containment measures should be promoted to reduce the impact of possible outbreaks. The strong dependence of R^2 on human mobility (see sensitivity analysis in the SI) points out the prominent role that human mobility plays in the dissemination of VBD and, therefore, its relevance for the design of efficient policies to prevent local outbreaks from spreading across populations.

Discussion

The control of infectious diseases represents one of the major societal challenges. Understanding the complex interdependency between human activity and contagion processes is key to explain the onset and development of large-scale epidemics. Here, focusing on VBD, we have integrated information from urban daily commutes and the geographic distribution of humans and vectors to estimate the epidemic risk associated to different connected regions. In particular, we have provided a metapopulation formalism to assess the role that the former ingredients play on the propagation of VBD. We have proved that this formalism constitutes a very reliable and time-saving platform, since its Markovian equations enable to reproduce very accurately not only the global incidence of VBD but also the spatio-temporal spreading patterns observed in Monte Carlo simulations.

Based on this agreement, we have derived an analytical expression of the epidemic threshold that captures the critical conditions which leads to the onset of epidemics. Apart from the detrimental effect that mobility may have on the spread of diseases, the study of the epidemic threshold has revealed interesting phenomena such the existence of abrupt changes in the way epidemics unfold. In particular, we have shown that the subset of patches leading the epidemic onset can suddenly change as human mobility varies. This phenomenon highlights the need of incorporating real human mobility patterns into the design of containment policies targeting specific geographical areas, for efficient policies can turn useless due to a small variation of human mobility habits.

Finally, relying on the matrix containing the information about the effective number of human-human contagions, we have derived an epidemic risk indicator that allows us to classify the patches according to their exposure to VBD. By computing this epidemic indicator, we have reproduced with great accuracy the geographical distribution of Dengue incidence in the city of Santiago de Cali (Colombia), where Dengue is an endemic disease, thus being able to identify the most vulnerable areas where prevention measures should be promoted.

In a nutshell, our results point out that the spread of VBD is the result of a delicate interplay between commuting flows, human census and vector distribution. This interplay is captured both in the analytical expression of the epidemic threshold and in the epidemic risk indicator. As a result of it, we have shown that small variations of the former ingredients, such as the degree of mobility, can lead to abrupt changes in the way epidemics unfold. Our framework, although containing several simplifying assumptions to allow the analytical treatment, has shown useful to integrate human and contagion dynamics and it can be readily implemented to identify those regions where immunization policies should be reinforced and to forecast the consequences of control strategies focused on mobility restrictions.

Methods

Mechanistic numerical simulations

With the aim of assessing the accuracy of the Markovian formulation we compared the predictions obtained using Eqs. 2-8 –for both the epidemic incidence and the spatio-temporal evolution of the disease– with numerical results from extensive mechanistic simulations.

In the simulations with synthetic networks we start by setting the human population of each node (n_i) to a constant value ($n_i = 10^3$), while vectors population m_i is set to be proportional to n_i as ($m_i = \gamma_i n_i$) with γ_i varying from one population to another and extracted from a uniform distribution within the range $\gamma_i \in [0.3, 1.7]$. For the mobility network of the city of Cali instead, we set n_i and m_i according to census and mosquitos proxy data publicly available from the municipality of Cali (see the SI for details). All the populations are initially composed only by healthy individuals until a seed of the disease is introduced in the system. For the seed we consider two different options: one in which the 1% of the agents in each sub-population is initially infected and a second one where the seed is localized in a single sub-population.

After the seed is introduced, the reactive and diffusive processes take place with the same time-scale. At each time step, agents decide whether to move to a neighboring patch or to remain in their home patch. To do so, each agent generates an independent and identically distributed random variable (i.i.d.) r between $[0, 1]$. If r is smaller than the moving probability p the agent will move otherwise, she will stay in her node. In addition, to model the possible impairment produced by the disease, we also assume that infected individuals could be less prone to move by rescaling their mobility to αp , with $0 \leq \alpha \leq 1$. In any case, if the agents moves, another i.i.d. r' determines the destination patch. r' is extracted between $[0, \sum_j W_{ij}]$, where W_{ij} is the weight of the link between populations i and j . Then, the destination is chosen as the first node k that satisfies $\sum_k W_{ik} \geq r'$, assuring that the destination is selected proportionally to the mobility flux between sub-populations i and k .

Once the agents reached their new location, an iteration of the contagion and recovery process starts. To model the infection dynamics of VBD inside each patch we rely on the Ross-Macdonald model on well mixed populations. Inside each population, each vector, regardless of its state, bites β randomly selected individuals. In the case that the vector is infected and the human is healthy the disease will spread with probability λ_{MH} . In the opposite case, the vector gets the disease with probability λ_{HM} . Finally, if the vector and the human are both healthy or both infected, nothing happens. Regarding the recovery phase, each infected human recovers with probability μ_H while mosquitos do not recover but are replaced by healthy new individuals at rate μ_M .

Simulations finish when the epidemic reaches a stationary state: i.e. or the disease dies out or the fluctuations in the total number of infected humans in the system $\rho^H(t)$ are lower than 10^{-5} during the last 100 time steps. Results are then averaged over the different realizations and compared with the theoretical predictions given by the Markovian model.

Synthetic Metapopulations

Synthetic metapopulations used in Fig. 2 are composed of 50 patches that correspond to the nodes of a network constructed following the preferential attachment model of Barabási and Albert⁵⁴ with mean degree $\langle k \rangle = 4$. The elements of matrix \mathbf{R} are: $R_{ij} = 1/k_i$, being k_i the degree of patch i . The human population of nodes are identical $n_i = 10^3$ while vector populations are randomly assigned in the range $m_i \in [300, 1700]$.

Contributions

All of the authors designed research. D.S.-P., J.H.A.-C., S.M. and J.G.-G. conducted research. J.H.A.-C. and H.J.M. provided and analyzed data. D.S.-P., S.M. and J.G.-G. wrote the manuscript. All the authors revised and approved the manuscript.

Competing financial interests

The authors declare no competing financial interests.

Acknowledgements

We are especially grateful to A. Arenas and O. Vasilieva for useful comments and discussions. This work was partially supported by Universidad del Valle (grant CI-165), Gobierno de Aragon/Fondo Social Europeo (Grant E36-17R), Ministerio de Economia, Industria y Competitividad (MINECO) and Fondo Europeo de Desarrollo Regional (FEDER) (Grants FIS2015-71582-C2 and FIS2017-87519-P) and by the Agencia Estatal de Investigacion (AEI, Spain) and Fondo Europeo de Desarrollo Regional under Project PACSS Project No. RTI2018-093732-B-C22 (MCIU, AEI/FEDER,UE) and through the María de Maeztu Program for units of Excellence in R&D (MDM-2017-0711 to IFISC Institute).

References

1. *Zika situation report*, World Health Organization Tech. Rep. (2016).
2. *A global brief on vector-borne diseases*, World Health Organization (2014).
3. *The world health report 2004 – changing history*, World Health Organization (2004).

4. M.U.G Kraemer *et al.*, The global distribution of the arbovirus vectors *Aedes aegypti* and *Ae. albopictus*. *Elife* **4**, e08347 (2015).
5. P. Reiter, Global warming and mosquito-borne disease in USA. *Lancet* **348**, 622 (1996).
6. S. Hales, N. de Wet, J. Maindonald, and A. Woodward. Potential effect of population and climate changes on global distribution of dengue fever: an empirical model. *Lancet* **360**, 830 (2002).
7. P. Reiter, Climate change and mosquito-borne disease: knowing the horse before hitching the cart. *Rev. Sci. Tech.* **27**, 383–398 (2008).
8. *Global vector control response 2017–2030*, World Health Organization (2017).
9. V. Colizza, A. Barrat A, M. Barthélemy, and A. Vespignani. The role of the airline transportation network in the prediction and predictability of global epidemics. *Proc. Nat. Acad. Sci. USA* **103**, 2015–2020 (2006).
10. B. Adams, and D.D. Kapan. Man bites mosquito: understanding the contribution of human movement to vector-borne disease dynamics. *PLoS One* **4**, e6763 (2009).
11. R. Guimerá, S. Mossa, A. Turtschi, and L. A. N. Amaral. The worldwide air transportation network: Anomalous centrality, community structure, and cities' global roles. *Proc. Nat. Acad. Sci (USA)* **102** 7794–7799 (2005).
12. M.C. Gonzalez, C.A. Hidalgo, A.L. Barabasi. Understanding individual human mobility patterns. *Nature* **453** (7196), 779 (2008).
13. M. Lee, H. Barbosa, H. Youn, P. Holme and G. Ghoshal. Morphology of travel routes and the organization of cities. *Nature Comm.* **8** 2229 (2017).
14. H. Barbosa, *et al.* Human mobility: Models and applications. *Phys. Rep.* **734** 1-74 (2018).
15. M. Akbarzadeh, and E. Estrada. Communicability geometry captures traffic flows in cities. *Nature Hum. Bev.* **2** 645–652 (2018).
16. I. Hanski. Metapopulation dynamics. *Nature* **396**, 41–49 (1998).
17. I. Hanski, and M.E. Gilpin. *Metapopulation Biology: Ecology, Genetics, and Evolution*. (Academic Press, 1997).
18. D. Tilman and P. Kareiva. *Spatial Ecology*. (Princeton University Press, 1997).
19. L. Sattenspiel, and K. Dietz. A structured epidemic model incorporating geographic mobility among regions. *Mathematical Biosciences* **128**, 71–91 (1995).
20. B. Grenfell, and J. Harwood. (Meta)population dynamics of infectious diseases. *Trends in Ecology & Evolution* **12**, 395–399. (1997).
21. V. Colizza, R. Pastor-Satorras, and A. Vespignani. Reaction–diffusion processes and metapopulation models in heterogeneous networks. *Nature Phys.* **3**, 276–282 (2007).
22. V. Colizza, and A. Vespignani. Invasion threshold in heterogeneous metapopulation networks. *Phys. Rev. Lett.* **99**, 148701 (2007).
23. V. Colizza, and A. Vespignani. Epidemic modeling in metapopulation systems with heterogeneous coupling pattern: Theory and simulations. *Journal of theoretical biology* **251**, 450–467 (2008).
24. D. Balcan, V. Colizza, B. Gonçalves, H. Hao, J.J. Ramasco, and A. Vespignani. Multiscale mobility networks and the spatial spreading of infectious diseases- *Proc. Nat. Acad. Sci (USA)* **106**, 21484–21489 (2009).
25. S. Altizer, A. Dobson, P. Hosseini, P. Hudson, M. Pascual, and P. Rohani. Seasonality and the dynamics of infectious diseases. *Ecology Letters* **9**: 467–484 (2006).
26. M. J. Keeling, P. Rohani. *Modeling infectious diseases in humans and animals*. (Princeton University Press, 2011).
27. S. Eubank, *et al.* Modelling disease outbreaks in realistic urban social networks. *Nature* **429**, 180–184 (2004).
28. D. Balcan, B. Goncalves, H. Hu, J. J. Ramasco, V. Colizza and A.Vespignani. Modeling the spatial spread of infectious diseases: The GLocal Epidemic and Mobility computational model. *Journal of Computational Science* **1**, 132–145 (2010).
29. M. Tizzoni *et al.* Real-time numerical forecast of global epidemic spreading: case study of 2009 A/H1N1pdm. *BMC Medicine* **10** 165 (2012).
30. F. Ball *et al.* Seven challenges for metapopulation models of epidemics, including households models. *Epidemics* **10**, 63–67 (2015).

31. N. M. Ferguson *et al.* (2005) Strategies for containing an emerging influenza pandemic in Southeast Asia. *Nature* **437**, 209–214.
32. J. Truscott, and N. M. Ferguson (2012) Evaluating the adequacy of gravity models as a description of human mobility for epidemic modeling. *PLOS Comput Biol* **8**(10) e1002699.
33. D. Balcan, and A. Vespignani. Phase transitions in contagion processes mediated by recurrent mobility patterns. *Nature Phys.* **7**, 581–586 (2011).
34. V. Belik, T. Geisel and D. Brockmann. Natural Human Mobility Patterns and Spatial Spread of Infectious Diseases. *Phys. Rev. X* **1**, 1, 011001 (2011).
35. D. Balcan, and A. Vespignani. Invasion threshold in structured populations with recurrent mobility patterns. *J. Theor. Biol.* **293**, 87–100 (2011).
36. J. Gómez-Gardeñes, D. Soriano-Paños, and A. Arenas. Critical regimes driven by recurrent mobility patterns of reaction-diffusion processes in networks. *Nature Phys.* **14**, 391-395 (2018).
37. J.T. Matamalas, M. De Domenico, and A. Arenas. Assessing reliable human mobility patterns from higher order memory in mobile communications. *J. R. Soc. Interface* **13**, 20160203 (2016).
38. D. Soriano-Paños, L. Lotero, A. Arenas, and J. Gómez-Gardeñes. Spreading processes in multiplex metapopulations containing different mobility networks. *Phys. Rev. X* **8**, 031039 (2018).
39. Y. Xiao, and X. Zou, Transmission dynamics for vector-borne diseases in a patchy environment. *J. Math. Biol.* **69**, 113–146 (2014).
40. O. Prosper, N. Ruktanonchai, M. Martcheva, Assessing the role of spatial heterogeneity and human movement in malaria dynamics and control. *J. Theor. Biol.* **303**, 1 (2012).
41. P. Auger, E. Kouokam, G. Sallet, M. Tchuente, B. Tsanou. The Ross-Macdonald model in a patchy environment, *Math Biosci.* **216**, 123 (2008).
42. D. L. Chao, I. M. Longini Jr, & M. E. Halloran (2013) The effects of vector movement and distribution in a mathematical model of dengue transmission. *PloS one*, **8**(10), e76044.
43. C. Cosner, J.C. Beier, R.S. Cantrell, D. Impoinvil, L. Kapitanski, M.D. Potts, A. Troyo, and S. Ruan, The effects of human movement on the persistence of vector-borne diseases. *J. Theor. Biol.* **258**, 550–560 (2009).
44. D. Moulay, and Y. Pigné, A metapopulation model for chikungunya including populations mobility on a large-scale network. *J. Theor. Biol.* **318**, 129–139 (2013).
45. A. Wesolowski, N. Eagle, A. J. Tatem, D. L. Smith, A. M. Noor, R. W. Snow, & C. O. Buckee (2012) Quantifying the impact of human mobility on malaria. *Science* **338**(6104), 267-270.
46. Q. Zhang *et al.*, Spread of Zika virus in the Americas. *Proc. Natl. Acad. Sci. U S A.* **114**, E4334 (2017).
47. G. España *et al.*, Exploring scenarios of Chikungunya mitigation with a data-driven agent-based model of the 2014-2016 outbreak in Colombia. *Sci. Rep.* **8**, 12201 (2018).
48. A. Allard, B. M. Althouse, S. V. Scarpino, and L. Hébert-Dufresne. Asymmetric percolation drives a double transition in sexual contact networks. *Proc. Natl. Acad. Sci. U S A.* **114**(34) 8969–8973 (2017).
49. A. Allard, B. M. Althouse, L. Hébert-Dufresne, and S. V. Scarpino. The risk of sustained sexual transmission of Zika is underestimated. *PLOS Pathogens* **13**(9): e1006633 (2017).
50. L.E. Muir, and B.H. Kay. *Aedes aegypti* survival and dispersal estimated by mark-release-recapture in northern Australia. *Am J Trop Med Hyg.* **58**, 277-282 (1998).
51. G. Escobar-Morales, *Cali en Cifras 2013* (Departamento Administrativo de Planeación, Santiago de Cali, 2013).
52. C.P. Mora-Aguirre, G. Perlaza, S. Duque-Rodriguez, M.F. Rueda, G.V. Martinez, and J. Holguin Ruiz, ASIS report (2016).
53. H.A. Suárez, E. Castillo, and J.H. Rojas, Boletines Epidemiológicos de enfermedades transmitidas por vectores sem. 52 (2014–2016).
54. A.L. Barabási and R. Albert, Emergence of scaling in random networks. *Science* **286**, 509–512 (1999).

Supplementary information

Contents

S1	Ross-Macdonald model	12
S2	Description of the Cali dataset	15
S3	Validation of the Markovian equations	16
S4	Linearization of the Markovian Equations	18
S5	Heuristic approximation of the epidemic threshold	20
S6	Consequences of the abrupt changes in the patches driving VBD	23
S7	Epidemic risk indicators: Synthetic and real metapopulations	23
S8	Range of validity	26
	References	26

S1 Ross-Macdonald model

The Ross-Macdonald (RM) model¹⁻³ is one of the most paradigmatic benchmarks for the study of the transmission of vector-borne diseases (VBD). Although many modifications can be made to include ingredients that play a role in the evolution of VBD (such as the seasonal effects that influence the activity of vectors), it captures the essential processes leading to the unfold of a disease in well-mixed populations. In this sense, the RM model has proved to be a very insightful framework for characterizing VBD which do not confer immunity such as Dengue.

Here, we derive from first principles a slightly modified version of the original RM model which sets the foundation for the metapopulation model. First, we consider a closed population of both vectors and humans which are homogeneously mixed. The model assumes that vectors and humans can be either Susceptible of contracting the disease or Infected. The relevant variables are (i) the fraction of infected humans at time t , $\rho^H(t)$, and (ii) the fraction of infected vectors at time t , $\rho^M(t)$. The evolution of these variables is given by the elementary processes depicted in Fig. S1. Namely, Susceptible humans become Infected with probability λ^{MH} after being bitten by an infected vector while healthy vectors get the infection with probability λ^{HM} when interacting with an infected human. We also define β as the number of contacts each vector has with (healthy or infected) humans, *i.e.* the feeding rate of each vector. No direct human-human or vector-vector infections are allowed. On the other hand, infected humans and vectors become healthy with probabilities μ^H and μ^M , respectively. For humans, this probability is easily understandable as the inverse of the infectious period – the time that an infected requires to overcome the disease–. Considering vectors, this intuition fails since once they get infected they cannot get rid of the pathogen. However, as we are dealing with steady populations, μ^M encodes the renewal of vectors population. All vectors that die are assumed to be replaced by newborn susceptible ones. Considering the above processes (see also Fig. S1) we can write the following time

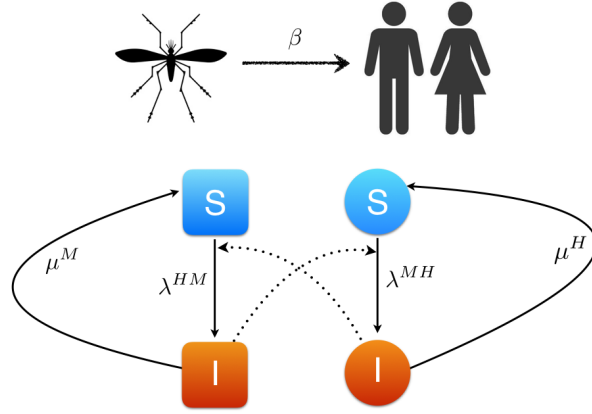


Figure S1. Schematic representation of the Ross-Macdonald model. Relevant parameters are: (i) the probability that an infected vector transmit the disease to a healthy individual, λ^{MH} , (ii) the probability that an infected human transmit the disease to a healthy vector, λ^{HM} , (iii) the feeding rate of a vector β , (iv) the probability that an infected human recovers, μ^H , and (v) the mortality rate of vectors, μ^M .

discrete dynamical equations for the fractions $\rho^H(t)$, and $\rho^M(t)$ as:

$$\rho^H(t+1) = \rho^H(t)(1 - \mu^H) + (1 - \rho^H(t))I^H(t), \quad (\text{S1})$$

$$\rho^M(t+1) = \rho^M(t)(1 - \mu^M) + (1 - \rho^M(t))I^M(t), \quad (\text{S2})$$

where N^H and N^M are the number of humans and vectors in the population respectively while $I^H(t)$ and $I^M(t)$ are the probabilities that a healthy human and a healthy vector get infected at time t , and they read as:

$$I^H(t) = \left[1 - \left(1 - \lambda^{MH} \rho^M(t) \frac{1}{N^H} \right)^{\beta N^M} \right], \quad (\text{S3})$$

$$I^M(t) = \left[1 - (1 - \lambda^{HM} \rho^H(t))^{\beta} \right]. \quad (\text{S4})$$

The first term in the r.h.s. of Eq. (S1) ((S2)) describes the fraction of infected humans (vectors) at time t who remains infected at time step $t + 1$ while the second term accounts for the fraction of healthy humans (vectors) that gets infected at time $t + 1$. Note also that Eq.(S3) includes an extra term with respect to Eq.(S4), that represents the probability for a human to receive a contact from each vector. We will demonstrate later that this element plays a crucial role on the unfolding of VBD.

Equations (S1) and (S2) can be reduced to the classical formulation of the RM model by taking into account that the terms $\lambda^{MH}\rho^M(t)$ and $\lambda^{HM}\rho^H(t)$ are pretty small so that, by using the approximated expression $1 - (1 - \varepsilon)^x \simeq x\varepsilon$, the continuous-time versions of Eqs. S1 and S2 turn into:

$$\dot{\rho}^H(t) = -\mu^H\rho^H(t) + \beta\lambda^{MH}\gamma(1 - \rho^H(t))\rho^M(t), \quad (\text{S5})$$

$$\dot{\rho}^M(t) = -\mu^M\rho^M(t) + \beta\lambda^{HM}(1 - \rho^M(t))\rho^H(t), \quad (\text{S6})$$

where γ is the ratio between the population of humans and vectors, $\gamma = \frac{N^M}{N^H}$, that can be considered as another parameter of the model.

Equations (S5) and (S6) represent the usual way the RM model is presented. As shown, they correspond to an approximation that turns to be valid close to the epidemic threshold, *i.e.*, when the fraction of infected vectors and humans are small but nonzero, while the formulation in Eqs. (S1-S4) is accurate in the entire epidemic diagram. The mathematical analysis of the model yields to an analytical estimation for the epidemic threshold as a function of the parameters λ^{MH} , λ^{HM} , μ^H , μ^M , β and γ . In particular, the first step to compute the threshold is to calculate the nullclines of the system of equations (S5) and (S6):

$$\dot{\rho}^H = 0 \rightarrow \rho^M = A \frac{\rho^H}{1 - \rho^H} \quad (\text{S7})$$

$$\dot{\rho}^M = 0 \rightarrow \rho^M = \frac{\rho^H}{B + \rho^H} \quad (\text{S8})$$

where $A = \frac{\mu^H}{\beta\lambda^{MH}\gamma} \geq 0$ and $B = \frac{\mu^M}{\beta\lambda^{HM}} \geq 0$. The above system is trivially satisfied by the $\rho^H = \rho^M = 0$, the case in which no prevalence of the virus is found in the system. However, we are interested in the stability of the epidemic phase.

From Eq. (S7) it becomes clear that ρ^M diverges as $\rho^H \rightarrow 1^-$ whereas Eq.(S8) reveal that ρ^M will continuously grow reaching $\rho^M = 1$ asymptotically. In Fig. S2 we plot the two nullclines (S7) and (S8) with solid (blue) and dashed (red) lines respectively. From the plot, it can be easily seen that the two curves cross for $\rho^H > 0$ only when the derivative of the dashed nullcline (S8) at ρ^H is larger than the one for the solid nullcline (S7). This condition is satisfied whenever

$$A < \frac{1}{B} \rightarrow \frac{1}{\gamma\beta^2} \frac{\mu^H\mu^M}{\lambda^{MH}\lambda^{HM}} < 1. \quad (\text{S9})$$

In this sense, the limit of this inequality determines the boundary between the epidemic and disease-free regimes. This boundary is given by the following equation:

$$\frac{\beta^2\lambda^{MH}\lambda^{HM}\gamma}{\mu^H\mu^M} = 1 \quad (\text{S10})$$

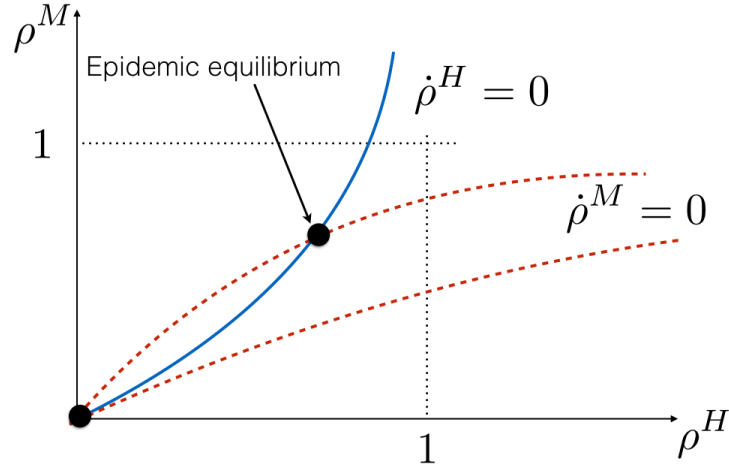


Figure S2. Graphical solution of the RM model. The solid (blue) line represents the nullcline of Eq. (S7) whereas the dashed (red) one is that of Eq. (S8). Besides the trivial solution at $\rho^H = \rho^M = 0$ the epidemic solution exists when the two nullclines intersect at $\rho^H > 0$.

S2 Description of the Cali dataset

One of the most important contributions of this work is the formulation of a new framework which can easily incorporate mobility data of real cities to address real epidemic scenarios. In the main text, we tackle the spread of VBD in the city of Cali (Colombia), whose geographical and meteorological features make it an endemic region for several VBD such as Dengue, Chikungunya or Zika. In particular, here we focus on the spread of Dengue.

To assess the effect of mobility on the spread of Dengue in Cali, it is necessary to reconstruct the mobility network of its inhabitants from data. For this purpose, we divide the city into 22 neighborhoods, which correspond to the official administrative divisions called *comunas*. Regarding demography, the population distribution across *comunas* has been extracted from census data that the municipality facilitates¹⁰. Mobility flows connecting *comunas* are extracted from urban commuting surveys⁸. As a result, more than 10^5 trajectories were recorded, which suppose a representative sample of Cali's commuting flows. Once data have been gathered, an origin-destination matrix, encoded in our formalism by matrix \mathbf{R} , is computed as:

$$R_{ij} = \frac{W_{ij}}{\sum_{l=1}^N W_{il}}, \quad (\text{S11})$$

where the numerator corresponds to the number of trips between patches i and j while the denominator counts all the reported trips departing from patch i . The result is a weighted directed network encoding the probability that an agent visits other neighborhoods different from its residence.

Apart from the mobility network, the distribution of vectors across the city also plays a crucial role on the outcome of the disease. The number of vectors inside a geographical region is strongly linked to environmental features such as altitude, temperature and humidity but also to human-dependent factors like health and economic conditions. To model vectors' distribution across patches, we use as a proxy the so-called *recipient index*⁴. This quantity encodes the probability of finding vector pupae in different recipients which have been previously distributed across the city. A high value of the index means a higher probability of finding vectors. For this reason, we assume that the ratio between the number of vectors and humans inside each patch in our model is directly proportional to its recipient index, which is extracted from a report published in 2014⁴.

S3 Validation of the Markovian equations

Here we aim at assessing the ability of our model to predict the impact of VBD in both synthetic and real world metapopulations. To do so, we compare theoretical predictions from our model with results from extensive mechanistic simulations. Theoretical predictions are obtained by iterating Eqs. (2-8) of the main text until a stationary state has been reached, while mechanistic simulations are performed by updating the dynamical state of vectors and humans following the dynamical rules defined in the main text (see *Methods*).

Let us first study the epidemic size –the fraction of the population who remains infected when the disease reaches a stationary state– as a function of the contagion rates between humans and vectors $\lambda^{MH}, \lambda^{HM}$ and mobility p . To reduce the number of parameters and without loss of generality, let us define $\lambda^{HM} = \lambda^{MH} = \lambda$. We start analyzing the case in which human mobility is governed by an unweighted undirected Barabási-Albert network (BA) of $N = 50$ patches (see *Methods*), all of them homogeneously populated by $n_i = 1000$ agents. Concerning vectors' distribution, we consider that the ratio between vectors and humans populations inside a patch i , denoted in the following as γ_i , is randomly drawn from a uniform distribution within the range $\gamma_i \in [0.3, 1.7]$. Figure S3 reveals the great agreement between theory and simulations for both the cases in which infected agents mobility is totally restrained, *i.e.* $\alpha = 0$ (Fig. S3a), and when there is no influence of the disease on agents' mobility, $\alpha = 1$ (Fig. S3b).

We now move to a real case, the city of Cali, whose metapopulation architecture is described in Sec. S2. Following the same procedure, we can notice in Fig. S3c-d that our formalism still captures very accurately the epidemic size, despite the higher complexity of Cali's mobility network. Apart from the agreement between theory and simulations, interesting physical phenomena arise from accounting for the mobility constraints associated with contracting severe VBD. In particular, we notice that the qualitative behaviour of the epidemic threshold with human mobility can drastically change when modifying the

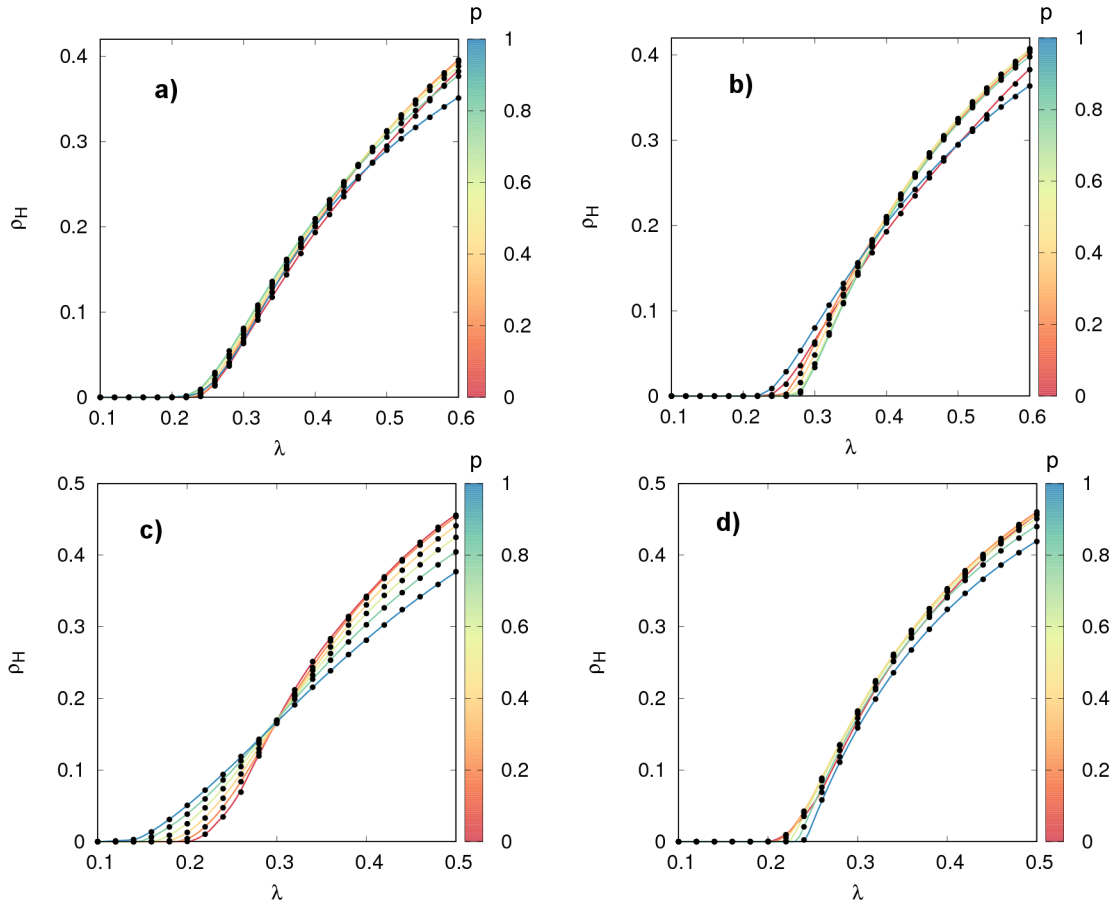


Figure S3. Epidemic size ρ_H as a function of the contagion rate between vectors and humans $\lambda^{HM} = \lambda^{MH} = \lambda$ and the human mobility p (color code). Dots correspond to results of averaging 25 stochastic realizations whereas solid lines represent the theoretical predictions obtained by iterating the equations of the formalism. The recovery rate for both humans and vectors is set to $\mu^H = \mu^M = 0.3$. Panels a)-b): The mobility network is the BA one described in the main text (see *Methods*). The values assumed for the restriction of the mobility of infected agents are (a) $\alpha = 0$ and (b) $\alpha = 1$. Panels c)-d): The network used is the mobility network of Cali previously described in Sec. S2 Section. The values of infected agents mobility restriction parameter are (c) $\alpha = 0$ and (d) $\alpha = 1$.

restriction parameter. These phenomena will be analyzed in more detail in the next section where we compute the epidemic threshold as a function of (p, α) .

Finally, we also want our theory to reproduce the spatio-temporal unfolding patterns of VBD across both synthetic and real networks. To check this, we start by setting a seed localized in a single patch, and then we monitor the temporal evolution of the population affected by the disease inside each area. Figure S4 reveals that our formalism is able to capture the different propagation pathways of VBD in the BA and Cali metapopulations, despite the noise induced by the stochastic nature of the mechanistic simulations.

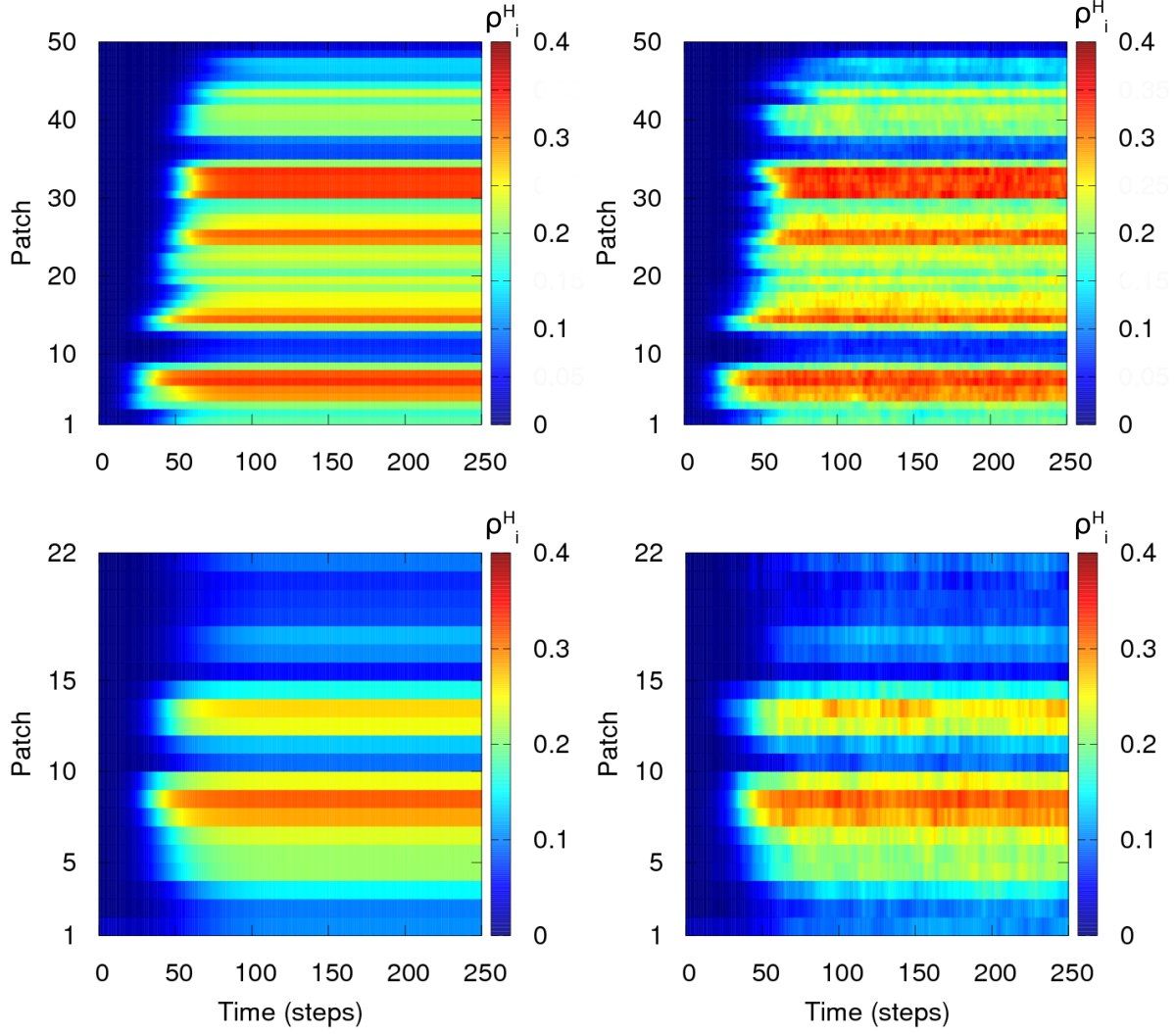


Figure S4. Temporal evolution of the fraction of infected agents (color code) inside each patch. Parameters values are $(\lambda, \mu^H, \mu^M, p, \alpha) = (0.3, 0.3, 0.3, 0.3, 0)$. Top panels: the metapopulation which governs mobility processes is synthetic one described in the main text (see Methods). Bottom: The metapopulation used is the Cali mobility network detailed in the previous Section. The left panels correspond to the iteration of Eqs.(2-8) whereas the right ones contain the results of a single Monte Carlo realization.

S4 Linearization of the Markovian Equations

Here we derive an analytical estimation of the epidemic threshold for the Ross-Macdonald model with metapopulations. In the main manuscript we have defined this quantity as the minimum infection rate from vectors to humans which leads to an epidemic regime in the stationary state. We start considering the steady state of the Markovian equations. Assuming $\rho_i^H(t+1) = \rho_i^H(t) = \rho_i^H$, $\rho_i^M(t+1) = \rho_i^M(t) = \rho_i^M \forall i$, Eqs. (2,3) of the main text turn into:

$$\mu^H \rho_i^H = (1 - \rho_i^H) I_i^H, \quad (\text{S12})$$

$$\mu^M \rho_i^M = (1 - \rho_i^M) I_i^M, \quad (\text{S13})$$

and the probabilities I^H and I^M that a human or a vector associated with node i becomes infected are respectively:

$$I_i^H = (1-p) \left[1 - \left(1 - \lambda^{MH} \rho_i^M \frac{1}{n_i^{eff}(\rho_H, \alpha, p)} \right)^{\beta m_i} \right] + p \sum_{j=1}^N R_{ij} \left[1 - \left(1 - \lambda^{MH} \rho_j^M \frac{1}{n_j^{eff}(\rho_H, \alpha, p)} \right)^{\beta m_j} \right]. \quad (S14)$$

$$I_i^M = 1 - \left(1 - \lambda^{HM} \frac{(1-\alpha p)n_i \rho_i^H + \alpha p \sum_{j=1}^N R_{ji} \rho_j^H}{n_i^{eff}(\rho_H, \alpha, p)} \right)^\beta. \quad (S15)$$

Close to the boundary between the epidemic and the disease-free phases, these steady values are small but not zero, which mathematically is reflected by considering $\rho_i^H = \varepsilon_i^H \ll 1$, $\rho_i^M = \varepsilon_i^M \ll 1 \forall i$. The latter allows us to linearize the equations by neglecting non-linear terms in ε . Thus, Eqs.(S14,S15) turn into:

$$I_i^H \simeq (1-p) \lambda^{MH} \beta m_i \frac{1}{n_i^{eff}(0, \alpha, p)} \varepsilon_i^M + p \sum_{j=1}^N R_{ij} \lambda^{MH} \beta m_j \frac{1}{n_j^{eff}(0, \alpha, p)} \varepsilon_j^M. \quad (S16)$$

$$I_i^M \simeq \beta \lambda^{HM} \left[\frac{(1-\alpha p)n_i \varepsilon_i^H}{n_i^{eff}(0, \alpha, p)} + \frac{\alpha p \sum_{j=1}^N R_{ji} n_j \varepsilon_j^H}{n_i^{eff}(0, \alpha, p)} \right]. \quad (S17)$$

We now introduce the former expressions into Eqs. (S12,S13) and keep only linear terms in ε , yielding:

$$\varepsilon_i^H = \sum_{j=1}^N \frac{\lambda^{MH} \beta}{\mu_H} \underbrace{\left(p R_{ij} \frac{m_j}{\tilde{n}_j^{eff}} + (1-p) \delta_{ij} \frac{m_i}{\tilde{n}_i^{eff}} \right)}_{M_{ij}} \varepsilon_j^M. \quad (S18)$$

$$\varepsilon_i^M = \sum_{j=1}^N \frac{\lambda^{HM} \beta}{\mu_M} \underbrace{\left(\alpha p R_{ji} \frac{n_j}{\tilde{n}_i^{eff}} + (1-\alpha p) \delta_{ij} \frac{n_i}{\tilde{n}_i^{eff}} \right)}_{\tilde{M}_{ij}} \varepsilon_j^H, \quad (S19)$$

where \tilde{n}_i^{eff} has been defined as $\tilde{n}_i^{eff} = n_i^{eff}(0, \alpha, p)$. For the sake of clarity, let us write the former system of equations in a more compact way:

$$\begin{pmatrix} \vec{\varepsilon}^H \\ \vec{\varepsilon}^M \end{pmatrix} = \begin{pmatrix} 0 & \frac{\beta \lambda^{MH}}{\mu^H} M \\ \frac{\beta \lambda^{HM}}{\mu^M} \tilde{M} & 0 \end{pmatrix} \begin{pmatrix} \vec{\varepsilon}^H \\ \vec{\varepsilon}^M \end{pmatrix}. \quad (S20)$$

Equation S20 makes evident the bipartite nature of the processes involved in the spread of VBD with matrices M and \tilde{M} responsible for vector-human and human-vector infections, respectively. Thus, if we want to quantify indirect infections between humans mediated by vectors and vice versa we should iterate Eq. S20 obtaining:

$$\begin{pmatrix} \vec{\varepsilon}^H \\ \vec{\varepsilon}^M \end{pmatrix} = \frac{\beta^2 \lambda^{MH} \lambda^{HM}}{\mu^M \mu^H} \begin{pmatrix} M \tilde{M} & 0 \\ 0 & \tilde{M} M \end{pmatrix} \begin{pmatrix} \vec{\varepsilon}^H \\ \vec{\varepsilon}^M \end{pmatrix}. \quad (S21)$$

From Eq. S21 it becomes clear that calculating the epidemic threshold involves solving an eigenvalue problem. In order to obtain a closed expression for the epidemic threshold and without loss of generality, we assume $\lambda^{MH} = \delta\lambda^{HM}$. Finally, as we are interested in the minimum value of λ^{HM} for which the former equation holds, the epidemic threshold can be estimated as:

$$\lambda_c^{MH} = \sqrt{\frac{\mu_H \mu_M}{\delta \beta^2 \Lambda_{max}(\mathbf{M}\tilde{\mathbf{M}})}}, \quad (\text{S22})$$

where Λ_{max} is the spectral radius of matrix $\mathbf{M}\tilde{\mathbf{M}}$.

S5 Heuristic approximation of the epidemic threshold

In the main text, we demonstrate that Eq. S22 accurately predicts the epidemic threshold. However, despite the accuracy of this estimation, its calculation involves computing the spectral radius of an arbitrarily large matrix which, for very extensive systems, can be a hard computational task. Here we derive a heuristic indicator that solves this problem and clarifies the intuition behind the different behaviors emerging as a result of human mobility.

Let us first discuss the physical meaning of Eqs. S16 and S17. Eq. S16 accounts for all the possible contagion processes affecting an agent with residence in i . Specifically, one agent associated with node i can become infected in two possible ways: staying at node i and getting bitten by a vector or moving to another sub-population and getting infected there. On the other hand, Eq. S17 counts the infectious interactions of a vector from i with agents that live there or belong to other patches and have decided to visit i . Thus, the number of indirect contagion processes C_i^2 received by a susceptible individual associated to a patch i from infected agents can be quantified by composing these cross contagion rates across all the patches of the metapopulation, *i.e.*:

$$C_i^2 = \frac{1}{\mu_H \mu_M} \beta^2 \delta (\lambda^{MH})^2 \sum_{j=1}^N \sum_{k=1}^N M_{ik} \tilde{M}_{kj}. \quad (\text{S23})$$

Therefore, the larger this quantity for patch i is, the higher the probability that an agent from i contracts the disease. Following this line, we can thus approximate the epidemic threshold as the minimum value of λ^{MH} needed to assure that an agent from the most exposed patch is infected at least once. This value, here defined as r^2 , is given by:

$$r^2 = \sqrt{\frac{\mu_H \mu_M}{\delta \beta^2 \max_i \left(\sum_{j=1}^N \sum_{k=1}^N M_{ik} \tilde{M}_{kj} \right)}}. \quad (\text{S24})$$

Fig. S5 shows a comparison between the epidemic threshold, calculated from the spectra of $\mathbf{M}\tilde{\mathbf{M}}$ (black line), and r^2 (blue dashed line) as a function of human mobility p for three different values of α . From Fig. S5, it can be observed that, regardless of α , r^2 approximates quite well the epidemic threshold for low mobilities, even the sharp variations due to the crossover

between the most affected areas. However, r^2 becomes less accurate when the mobility of infected and susceptible individuals are quite different.

To explain this discordance, we must take into account that, as infected individuals mobility is restrained, contagions between agents from different residences require more indirect contacts to happen. A very illustrative example is to consider two patches, say A and B, that are not mutually connected but both have connections to a third one, say C. If $\alpha = 1$ an infected agent from A can pass the disease to a healthy individual from B in two steps:

1. The infected agent moves to C and infects a vector there.
2. The infected vector bites a visitor from B, who becomes infected.

However, for $\alpha = 0$, this cannot happen since infected individuals are not allowed to move. In fact, now the shortest contagion path contains 4 steps:

1. The infected agent stays at A and a vector contracts the disease there.
2. A susceptible agent from C moves to A and becomes infected after being bitten.
3. This infected agent stays at C and transmits the disease to a vector there.
4. Finally, the infected vector at C passes the disease to the susceptible coming from B.

The latter example makes evident the necessity of considering contagion processes beyond two time steps to estimate the epidemic threshold. Following the same procedure as in the 2-step case, the number of indirect contagion processes that an agent from i receives in 4 steps can be calculated by:

$$C_i^4 = \frac{1}{\mu_H^2 \mu_M^2} \beta^4 \delta^2 (\lambda^{MH})^4 \sum_{ijklm}^N M_{ik} \widetilde{M}_{kl} M_{lm} \widetilde{M}_{mj}. \quad (\text{S25})$$

Therefore, the minimum λ^{MH} value to hold the epidemic, denoted as r^4 , is given by:

$$r^4 = \sqrt[4]{\frac{\mu_H^2 \mu_M^2}{\delta^2 \beta^4 \max_i \left(\sum_{ijklm}^N M_{ik} \widetilde{M}_{kl} M_{lm} \widetilde{M}_{mj} \right)}} \quad (\text{S26})$$

Finally, Fig. S5 demonstrates that r^4 (white dashed line) provides a better estimation for the threshold than r^2 , especially for high mobility values. As anticipated, this is mainly caused by the large number of contagious paths which are not captured by C_i^2 when the mobility of infected individuals is seriously constrained by the disease.

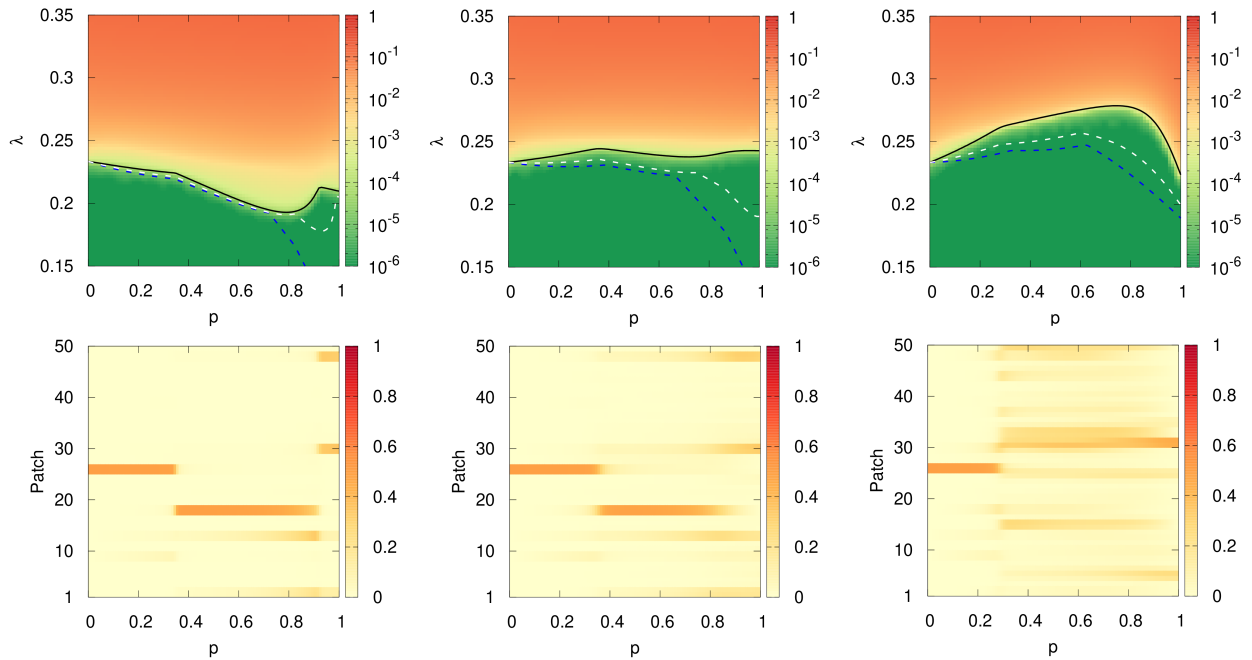


Figure S5. Epidemic size (color code) as a function of the infectivity $\lambda^{MH} = \lambda^{HM} = \lambda$ and mobility p . From left to right values of α used are $\alpha = 0, 0.5, 1$. Solid black line corresponds to the theoretical prediction for the epidemic threshold given by Eq. S22. Dashed lines represents the proposed indicators by taking into account 2-steps contagions (blue) and 4 steps ones (white). The remaining parameters have been set to $(\beta, \mu^H, \mu^M) = (1, 0.3, 0.3)$.

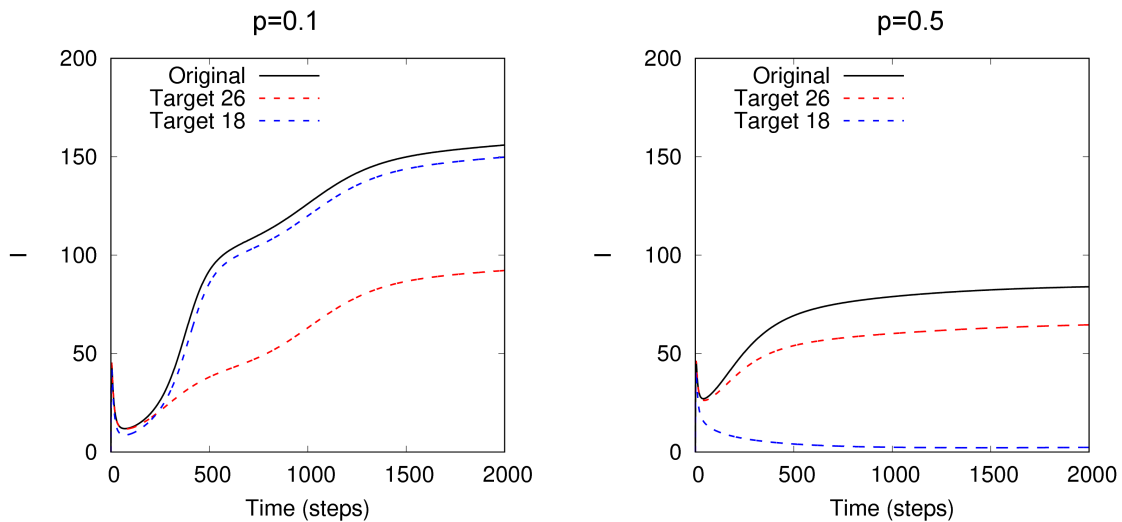


Figure S6. Temporal evolution, according to the Markovian equations, of the number of infected agents by a VBD which spreads over a BA network. The black line denotes the original curve where no policy has been implemented whereas dashed lines correspond to the case in which patches 26 (Red) and 18 (Blue) are immunized. The epidemic parameters have been set to $(\alpha, \lambda^{HM}, \lambda^{MH}, \mu^H, \mu^M) = (0.5, 0.25, 0.25, 0.3, 0.3)$. The values for human mobility are $p = 0.1$ ($p < p_c$ Left panel) and $p = 0.5$ ($p > p_c$ Right panel).

S6 Consequences of the abrupt changes in the patches driving VBD

The study of the critical properties of VBD in the main manuscript has revealed the existence of some mobility values, denoted as p_c , for which the components of the leading eigenvector change abruptly. Translated into epidemiological words, this striking phenomenon reflects the change in the most affected patches, which is of great relevance since targeted policies in specific areas can pass from useful to useless as human mobility varies. To prove it, we now study the effects of applying prevention measures in specific locations selected according to the largest components of the leading eigenvector of the critical matrix $\mathbf{M}\tilde{\mathbf{M}}$. We consider the synthetic network used in the main text and set $\alpha = 0.5$, for which the change in the leading patch happens at $p = p_c = 0.38$ (see Fig.2 in main manuscript). Finally, we target two different sub-populations for the immunization: patch 26 that is the leading patch for $p < p_c$, and patch 18 that sustains the outbreak for $p > p_c$.

Figure S6 confirms that the effectiveness of targeted policies against VBD is strongly influenced by aspects concerning human mobility. Thus, for example, immunizing agents from patch 18 leads to the extinction of the disease for $p > p_c$, whereas it is almost ineffective for mobility values below this threshold. This result, along with the others presented in the main text, highlights the importance of promoting containment policies not only based on demography or entomological information but also taking into account the complex interplay between human movement, census data and vector abundance.

S7 Epidemic risk indicators: Synthetic and real metapopulations

In the previous section, we proposed two heuristic indicators $-C_i^2$ and C_i^4 —able to capture, not only the dependence of the epidemic threshold on the mobility, but also changes in the patches driving the onset of epidemics. Here we go one step further and provide a prevalence indicator able to reproduce the spatial distribution of the disease across sub-populations. Our aim is to classify the different geographical areas according to the risk associated to VBD. To do so, let us recall that C_i^2 encodes all the possible indirect infectious contacts that an agent from i receives during an outbreak. Therefore, to obtain an estimate of the disease incidence in each patch, we must also account for the population of each geographical area. This way, we can define an epidemic risk indicator ER_i for each patch i as:

$$ER_i = n_i \sum_{j=1}^N \sum_{k=1}^N M_{ik} \widetilde{M}_{kj} \quad (\text{S27})$$

At this point, it is important to notice that Eq. S27 does not depend on the epidemiological traits of the disease but only on human census, mobility and mosquitos abundance. In fact, as we assume all the epidemiological parameters to be constant across all the areas, dealing with one or another disease only leads to a rescaling of the epidemic risk of all the regions without producing any change in the ranking of affected populations.

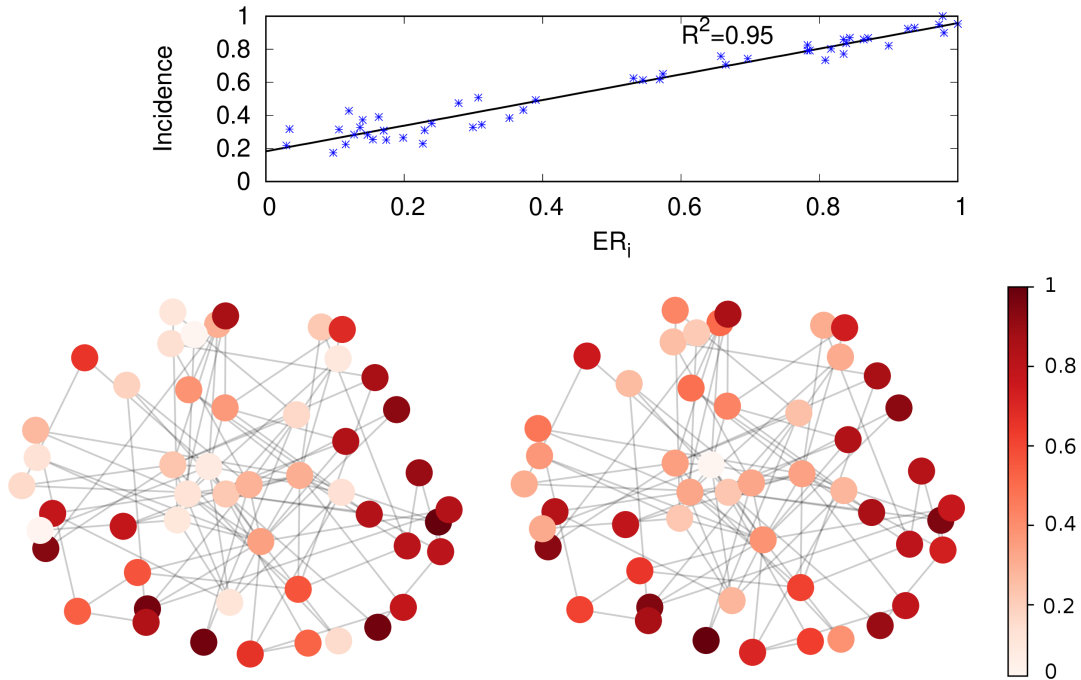


Figure S7. *Upper panel:* correlation between the epidemic risk indicator ER and the fraction of infected individuals in each patch given by the mechanistic simulations for a synthetic scale free network of 50 patches with $n_i = 10^3$ and $m_i \in [300, 1700]$. *Lower panel:* spatial comparison. The color code represents: on the left, disease incidence obtained in the numerical simulations while on the right, the epidemic risk indicator computed according to Eq. S27. The parameters for the simulations have been set to $(p, \alpha, \beta, \lambda^{MH}, \lambda^{HM}, \mu^H, \mu^M) = (0.2, 0.5, 1, 0.36, 0.36, 0.3, 0.3)$.

Synthetic metapopulations

We start testing the goodness of the predictions obtained via Eq. S27 in a controlled environment using a synthetic metapopulation. We compare its value for each patch with the incidence of the disease from lengthy mechanistic simulations on the synthetic network used in the main text. We then fix the epidemiological parameters (namely: the cross-contagion rates $\lambda^{MH}, \lambda^{HM}$, the vectors' biting rate β and the recovery rates μ^H and μ^M) as well as human mobility p and α while human population inside each patch is constant ($n_i = 10^3$) and vectors abundance is randomly assigned in the range $m_i \in [300, 1700]$. Figure S7 demonstrates the accuracy of our formalism in reproducing the unfolding of an outbreak in this controlled scenario, leading to a coefficient of determination $R^2 \simeq 0.95$.

Real metapopulations

We now check the applicability of our indicator to real scenarios. In particular, we focus on the spread of Dengue in the city of Cali in Colombia. Dengue constitutes an important threat for Cali inhabitants so local authorities monitor the situation and publish yearly reports^{5,6} with the spatial evolution of the disease across *comunas* and surveys about commuting inside the city

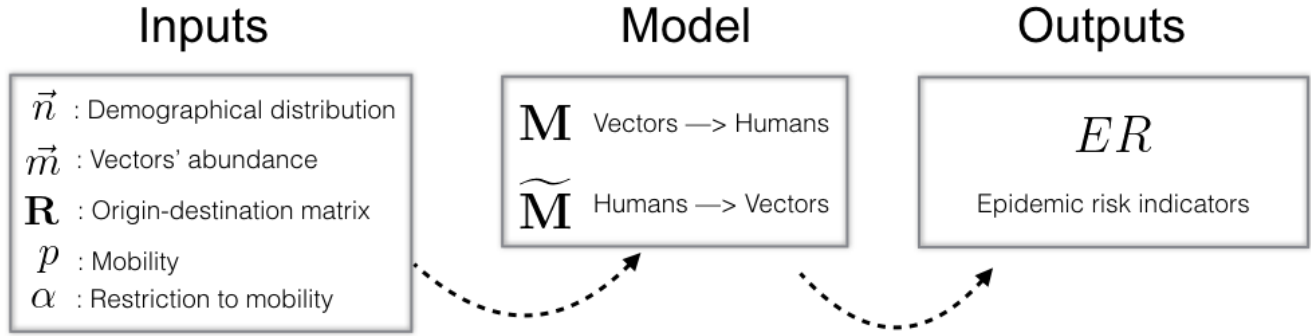


Figure S8. Steps needed to compute the epidemic risk indicator for each geographical area i . First, it is necessary to construct a metapopulation network from the demographical distribution, the vectors abundance and the observed origin destination trips. Second, by fixing the value of the mobility p as well as the restriction to the mobility of infected individuals α , we can estimate the critical matrices \mathbf{M} and $\tilde{\mathbf{M}}$. Finally, we compute the epidemic risk indicators ER_I using Eq. S27

are openly available⁸.

From the raw data only few steps are needed to compute the epidemic risk (see Fig S8). First, we should build the metapopulation systems. The inputs required are the demographical distribution \vec{n} , the vectors' abundance \vec{m} and the recurrent mobility patterns encoded in the matrix \mathbf{R} . Demographical distributions can be easily extracted from census published by local authorities – in the case of Cali we extracted them from reports issued by the Municipality¹⁰ – while vectors' abundance can be inferred from entomological indexes associated to each area such as the recipient index or the pupae index. Finally, different methods have been proposed to estimate the origin-destination matrix \mathbf{R} , which range from theoretical models⁷ to the realization of surveys⁸ or the use of mobile phone call records⁹.

With the structure and mobility of the metapopulation system fixed, we can compute the entries of matrices \mathbf{M} and $\tilde{\mathbf{M}}$, which depend also on the parameters related to human mobility α, p . To estimate α we recall that it represents the restriction in human mobility of infected individuals due to the effects of the disease. As symptoms associated with Dengue are usually severe, we can assume that all the symptomatic patients will not move, so α can be estimated as the percentage of asymptomatic infections that are $\sim 75\%$ of the infected population in case of Dengue disease. In its turn, the mobility p can be estimated as the fraction of individuals departing from their residence every day. Once defined the mobility, we can compute \mathbf{M} and $\tilde{\mathbf{M}}$ by using Eqs. S16 and S17 respectively. Finally, the epidemic risk is easily obtained by including these matrices in Eq. S27.

The results of the comparison have been shown in Fig. 3 of the main text, where we compare the epidemic risk indicator with the spatial distribution of Dengue cases in Cali from 2015 to 2016. For this particular scenario, the mobility value p is chosen to optimize the correlation between data and theory, yielding $p = 0.36$. The good agreement between theoretical indicator and the real cases ($R^2 = 0.81$) supports again the goodness of our approach, especially in presence of noisy and

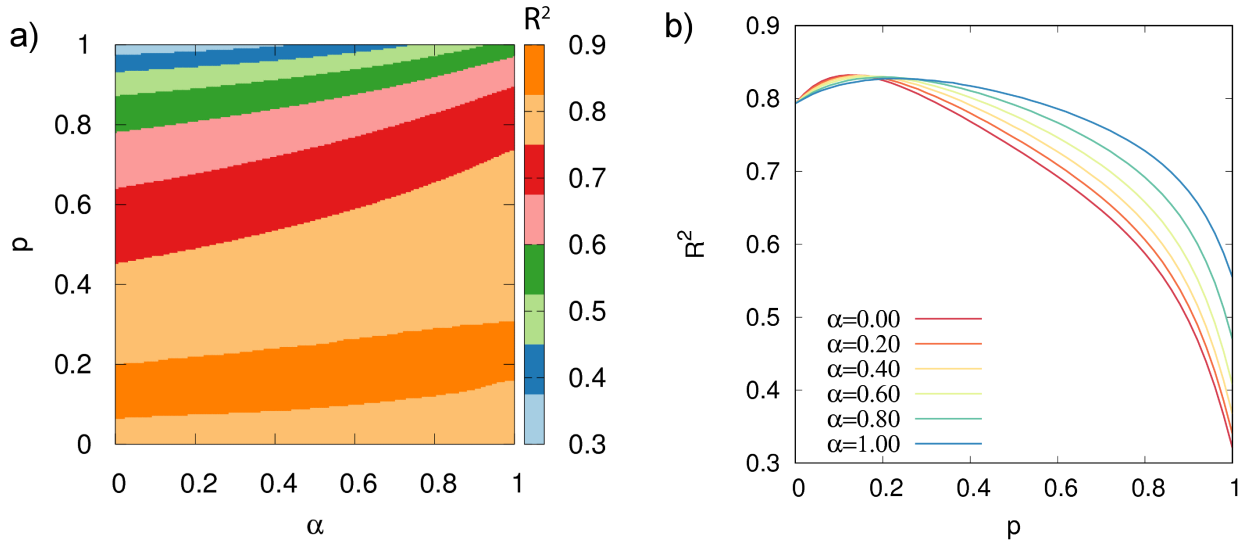


Figure S9. (a) Coefficient of determination R^2 (color code) as a function of the degree of mobility p and the infected individuals mobility α . (b) R^2 as a function of the mobility p for several values of α .

incomplete information, and its applicability to real world scenarios with the need of only few, and usually available, data.

S8 Range of validity

In the previous section, we have shown the accuracy of ER_i while considering both real and synthetic metapopulations. However, as mentioned above, its value depends on features related to human movements such as the degree of mobility p or the disease induced constraint of the mobility α . In this section we aim to test the robustness of ER_i under variations of these parameters and, therefore, to determine its range of validity.

To do so, we focus on the case of Cali and analyze the agreement between theory and the epidemiological data (quantified by R^2) as a function of both p and α . Fig. S9a shows us that R^2 remains over 0.80 for mobility values below $p = 0.5$ and practically the entire range of α . The agreement becomes more evident (see Fig. S9b) if we consider larger values of α as in the case of Dengue ($\alpha \simeq 0.75$) where $R^2 \leq 0.75$ for values of human mobility up to $p = 0.7$.

References

1. Ross R. The prevention of malaria (2nd ed.). (Murray, London), (1911).
2. Macdonald G. The epidemiology and control of malaria. (Oxford University Press, London) (1911).
3. Smith DL, Battle KE, Hay SI, Barker CM, Scott TW, McKenzie FE. Ross, Macdonald, and a Theory for the Dynamics and Control of Mosquito-Transmitted Pathogens. PLoS Pathog 8(4): e1002588.

4. Mora C, Duque S y Perlaza G. Analisis de Situación Integrado de Salud, municipio de Santiago de Cali. Secretaria de Salud Pública Municipal de Cali (2015).
5. Secretaría de Salud del Valle del Cauca. Boletin Epidemiologico. Valle del Cauca, Semana Epidemiologica n. 52 (2015).
6. Secretaría de Salud de Santiago de Cali. Boletin Epidemiologico. Cali, Semana Epidemiologica n. 39 (2016).
7. M. C. González, C. A. Hidalgo and A. L. Barabási. Understanding individual human mobility patterns. *Nature* **453**, 779 (2008).
8. Universidad Nacional de Colombia and AREA Metropolitana del Valle de Aburrá. Encuesta origen destino de viajes 2005 del Valle de Aburrá, estudios de tránsito complementarios y validación. Technical Report (2006).
9. M. Tizzoni *et al.* On the use of human mobility proxies for modeling epidemics. in *Plos. Comp. Bio.* **10**, e1003716 (2014).
10. G. Escobar-Morales, *Cali en Cifras 2013* (Departamento Administrativo de Planeación, Santiago de Cali, 2013).